PROCEEDINGS OF SCIENCE

Nucleon generalized form factors with twisted mass fermions

Constantia Alexandrou *
Department of Physics, University of Cyprus, P.O. Box 20537, 1678 Nicosia, Cyprus, and Computation-based Science and Technology Research Center, Cyprus Institute, 20 Kavafi Str., Nicosia 2121, Cyprus
E-mail: alexand@ucy.ac.cy

Martha Constantinou
Department of Physics, University of Cyprus, P.O. Box 20537, 1678 Nicosia, Cyprus
E-mail: constantinou.martha@ucy.ac.cy

Vincent Drach
NIC, DESY, Platanenallee 6, D-15738 Zeuthen, Germany
E-mail: vincent.drach@desy.de

Karl Jansen
NIC, DESY, Platanenallee 6, D-15738 Zeuthen, Germany
E-mail: karl.jansen@desy.de

Christos Kallidonis
Department of Physics, University of Cyprus, P.O. Box 20537, 1678 Nicosia, Cyprus, and Computation-based Science and Technology Research Center, Cyprus Institute, 20 Kavafi Str., Nicosia 2121, Cyprus
E-mail: kallidonis.christos@ucy.ac.cy

Giannis Koutsou
Computation-based Science and Technology Research Center, Cyprus Institute, 20 Kavafi Str., Nicosia 2121, Cyprus
E-mail: g.koutsou@cyi.ac.cy

We present results on the nucleon form factors, momentum fraction and helicity moment for $N_f = 2$ and $N_f = 2+1+1$ twisted mass fermions for a number of lattice volumes and lattice spacings. First results for a new $N_f = 2$ ensemble at the physical pion mass are also included. The implications of these results on the spin content of the nucleon are discussed taking into account the disconnected contributions at one pion mass.

31st International Symposium on Lattice Field Theory - LATTICE 2013
July 29 - August 3, 2013
Mainz, Germany

*Speaker.

PoS(LATTICE 2013)292

1. Introduction

Fundamental properties of the nucleon such as its charge radius, magnetic moment and axial charge have been studied experimentally for over 50 years. This work focuses in computing these fundamental properties within the lattice QCD formulation using twisted mass fermions (TMF). Several $N_f = 2$ and $N_f = 2+1+1$ ensembles generated at three different lattice spacings smaller than 0.1 fm [1, 2] are analyzed [3]. The twisted mass formulation is particularly suited for hadron structure calculations since it provides automatic $\mathcal{O}(a^2)$ improvement requiring no operator modification [4]. Our results include a simulation using the Iwasaki gluon action, and $N_f = 2$ TMF with a clover term at the physical value of the pion mass, referred to as the physical ensemble [5].

2. Setting scale

For baryon observables we opt to set the scale by using the nucleon mass at the physical limit. In Fig. 1 we collect all the data on the nucleon mass, including our new result using $N_f = 2$ the physical ensemble. As it can be seen, all data fall nicely on a universal curve.

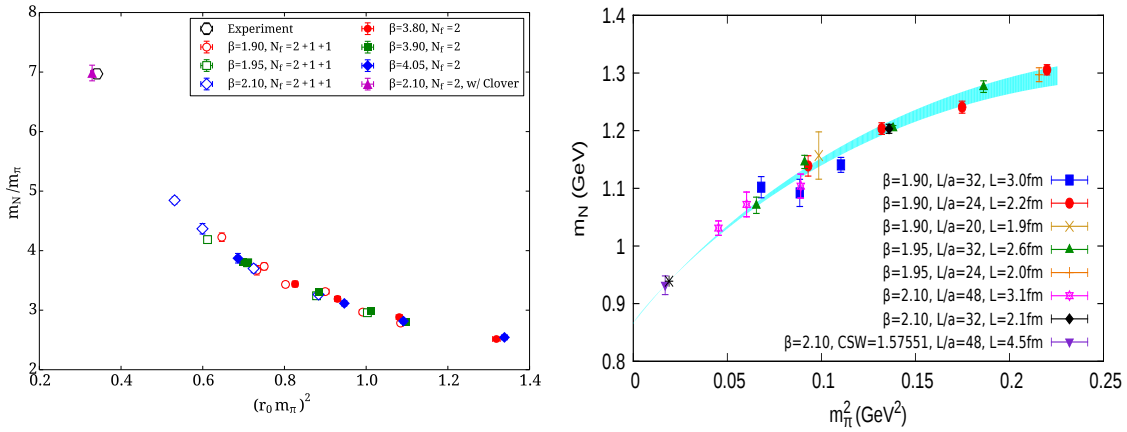

Figure 1: Left: The ratio of the nucleon mass to the pion mass versus $(m_\pi r_0)^2$. Right: Chiral extrapolation of the nucleon mass to extract the lattice spacings.

The physical pion mass is expressed in units of r_0 the value of which is determined from the nucleon mass. Restricting to the $N_f = 2+1+1$ ensembles generated with pion mass less than 300 MeV and including the physical ensemble we find $r_0 = 0.495(6)$ fm. In order to fix the lattice spacing a, we make a combined fit to the $N_f = 2+1+1$ ensembles at $\beta = 1.9$, $\beta = 1.95$ and $\beta = 2.1$, and to the physical ensemble using the well-established baryon chiral perturbation theory result $m_N = m_N^0 - 4c_1 m_\pi^2 - \frac{3g_A^2}{16\pi f_\pi^2} m_\pi^3$. The systematic error due to the chiral extrapolation is estimated in two ways: i) using the next order result in heavy baryon chiral perturbation theory (HBχPT) that includes explicit Δ-degrees of freedom, and ii) varying the pion mass range for the fit. In performing a combined fit we assume that cut-off effects are negligible. By fitting the results at each β-value separately we obtain consistent values, thus verifying the smallness of cut-off effects. From the combined fit, we obtain $a = 0.0936(13)(25)$ fm, $a = 0.0823(11)(35)$ fm, $a = 0.0646(7)(25)$ fm for $\beta = 1.90$, 1.95 and 2.10 for the $N_f = 2+1+1$ ensembles and $a = 0.0937(2)(2)$ fm for our

$N_f = 2$ physical ensemble. The lowest order chiral fit is shown in Fig. 1 and describes well all lattice QCD data. The lattice spacings for the $N_f = 2$ ensembles were similarly determined and given in Ref. [6]. The Feynman-Hellman theorem relates the coefficient c_1 of the p^3 fit to the $\sigma_{\pi N}$-term. Using the value of c_1 from our combined fit we find $\sigma_{\pi N} = 58(8)(7)$ MeV [7].

3. High precision study of nucleon observables at $m_\pi = 373$ MeV

In order to study excited state contributions, we perform a high-statistics study using one $N_f = 2+1+1$ ensemble at $\beta = 1.95$ and pion mass $m_\pi = 373$ MeV, referred to as B55.32. We focus on three observables chosen because they show a different degree of excited states contamination, namely the nucleon axial charge g_A where they are expected to be small, the isovector momentum fraction $\langle x \rangle_{u-d}$ where we expect them to contribute [8] and the scalar charge or equivalently the σ-terms where we expect severe contamination [9]. We also use this ensemble to compute the disconnected contributions to all nucleon observables with techniques reported in Ref. [10].

As customary, we construct an appropriate ratio of the three-point function we are interested in to two point functions, which for zero momentum transfer is given by $R(t_s, t_{\rm ins}) = \frac{G^{\rm 3pt}(\Gamma^\mu, t_s, t_{\rm ins})}{G^{\rm 2pt}(\Gamma^0, t_s)}$. We perform two types of analysis for the extraction of the matrix element: i) In the so-called plateau method we study the large Euclidean time evolution of the ratio

$$R(t_s, t_{\rm ins}) \xrightarrow[(t_s - t_{\rm ins})\Delta \gg 1]{(t_{\rm ins})\Delta \gg 1} \mathscr{M}[1 + \ldots e^{-\Delta(\mathbf{p}) t_{\rm ins}} + \ldots e^{-\Delta(\mathbf{p}')(t_s - t_{\rm ins})}] \tag{3.1}$$

where $\mathscr{M}$ is the desired matrix element, t_s and $t_{\rm ins}$, the sink and insertion separation time (we have taken the time of the source $t_0 = 0$), and $\Delta(\mathbf{p})$ the energy gap between the first excited state and the ground state. In the second approach the ratio is summed over $t_{\rm ins}$:

$$\sum_{t_{\rm ins}=t_0}^{t_s} R(t_s, t_{\rm ins}) = \text{Const.} + \mathscr{M}\,[t_s + \mathscr{O}(e^{-\Delta(\mathbf{p}) t_s}) + \mathscr{O}(e^{-\Delta(\mathbf{p}') t_s})]. \tag{3.2}$$

In this so-called summation method [11], excited state contributions are suppressed by exponentials decaying with t_s, rather than $t_s - t_{\rm ins}$ and $t_{\rm ins}$. However, one needs to fit the slope of the summed ratio rather than to a constant as in the plateau method. We note that this result also holds if one does not include t_0 and t_s in the sum, avoiding contact term contributions. All results shown here do not include these terms. We use the incremental eigCG algorithm [12] to speed-up the inversions at different t_s yielding a factor of 3 speed-up. We note that with one sequential inversion for each t_s we obtain results for all operator insertions.

The axial charge $\mathbf{g_A}$: The nucleon axial charge g_A, defined as the nucleon matrix element of the axial-vector current $A^3_\mu = \bar{\psi}\gamma_\mu\gamma_5\frac{\tau^3}{2}\psi$ at zero momentum transfer, is well-known experimentally and, being an isovector, receives no quark loop contributions. Therefore, it can be considered as the simplest baryon observable beyond the mass. In Fig. 2 we show the renormalized ratios $\tilde{R}(t_{\rm ins}, t_s)$ from which the isovector, and the isoscalar axial charge are determined for the B55.32 ensemble. We observe that the value of the plateau is the same for several t_s or equivalently no curvature is seen in the summed ratio, which yields the same slope either using initial fit time $t_i/a = 4$ or $t_i/a = 10$. This means that there is no detectable excited states contamination in the ratio yielding g_A even for $t_i/a = 4$, a result that corroborates our previous high precision study using the fixed current sequential method [8].

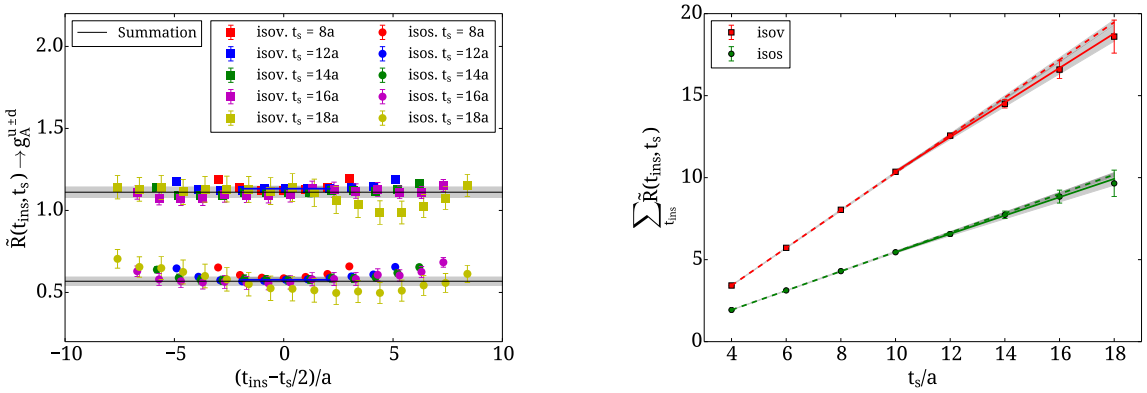

Figure 2: Left: $\tilde{R}(t_{\rm ins},t_s)$ for the isovector (squares) and connected isoscalar (circles) axial charge. The blue bands show the plateau-value for $t_s/a = 12$. The gray bands are the results extracted by fitting to the slope of the summed ratio as shown in the right panel. A total of 1200 measurements were used for each t_s.

The quark momentum fraction and the scalar charge: An analogous study is carried out for the quark momentum fraction $\langle x\rangle_{u-d}$ extracted from the nucleon matrix elements of $\mathcal{O}^{\mu_1\mu_2} = \bar{\psi}\gamma^{\{\mu_1} i \overleftrightarrow{D}^{\mu_2\}}\psi$ at momentum transfer squared $q^2 = 0$. Our results for the B55.32 ensemble are shown in Fig. 3. The renormalized ratio for $\langle x\rangle_{u-d}$ decreases as the sink-source separation increases. Fitting the plateau when $t_s/a = 18$ yields consistent results with those obtained from the summation method, for both the isovector and isoscalar quantities. Such agreement is what is expected when excited state contributions become negligible. The isoscalar charge $g_s^{u+d} = \langle N|\bar{u}u + \bar{d}d|N\rangle$ is computed in an analogous way to the calculation of the nucleon sigma-terms making use of the advantages of twisted mass fermions [9, 13]. The scalar and tensor charges, g_s and g_T, provide constrains for possible scalar and tensor interactions at the TeV scale [14]. In Fig. 3 we show the ratio from which the $\sigma_{\pi N}$ or equivalently the isoscalar scalar charge is extracted. Fitting at $t_s \sim 1.0$ fm will underestimate the scalar charge or $\sigma_{\pi N}$-term by 25%. Fitting the plateau and the summed ratio at large enough time separations yields consistent results. Thus consistency between the plateau and the summation method is a prerequisite for ascertaining that excited states contributions to the ratio are negligible.

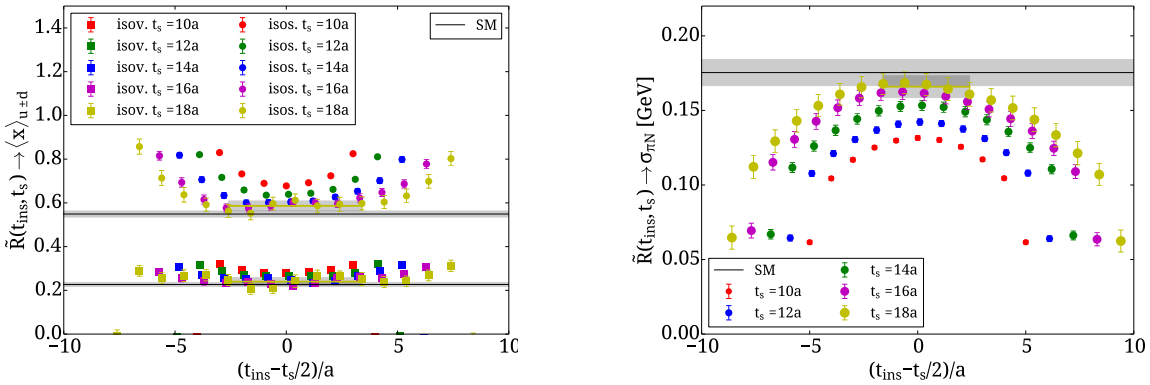

Figure 3: The ratio from which the isovector and connected isoscalar momentum fraction is extracted (left) and the corresponding ratio for $\sigma_{\pi N}$ (right). The notation is the same as that of Fig. 2.

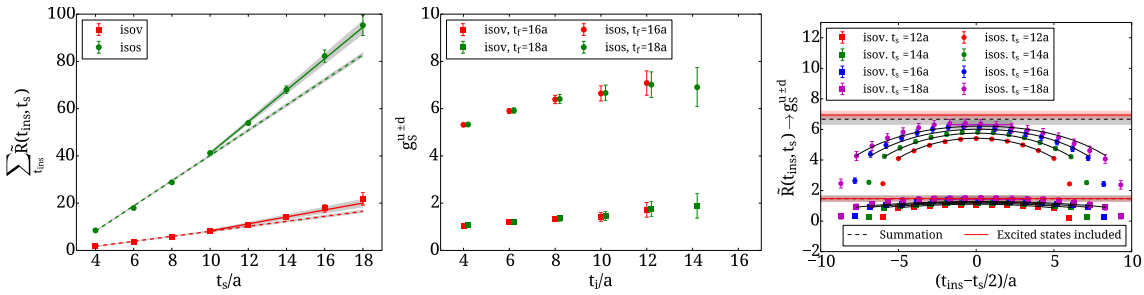

Figure 4: The summed renormalized ratio (left) and the slope (center) as a function of the initial fitting time t_i/a for two final fitting ranges $t_f/a = 16$ and $t_f/a = 18$. The solid lines in the right panel show the combined fit to results obtained for a number of t_s that explicitly includes the contributions of the first excited state.

In Fig. 4 we examine further the excited state contributions to the scalar charge. We show the dependence of the slope extracted from the summed renormalized ratio on the lower fit range t_i/a. Different values are obtained if we perform the fit using $t_i/a = 4$ as compare to using $t_i/a = 8$. Thus, just like in the plateau method, one seeks convergence of the slope as t_i increases, as shown in the center-plot in Fig.4. The value of the slope is not affected when changing the upper fitting range t_f/a from 16 to 18. We find that we need $t_i/a \geq 10$ to damp sufficiently excited state contributions. One can also include explicitly in the fitting function the terms due to the excited states. Taking into account the contributions of the first excited state and making a combined fit to all time separations using four fitting parameters yields consistent results, as demonstrated in Fig. 4. We stress that all methods to probe excited states require an evaluation of the three-point function for several sink-source time separations. For the scalar charge and $\sigma_{\pi N}$, one observes severe contamination from excited states requiring sink source separations of at least 1.5 fm. Agreement of summation, plateau and two-state fits give confidence to the correctness of the final result.

The isoscalar axial, momentum fraction and scalar charge have disconnected contributions, which need special techniques for their computation. We have calculated these contributions in Ref. [10] for the B55.32 ensemble using ∼150,0000 statistics on 4700 confs. We have found a non-zero result for g_A and g_s^{u+d}, which is about 10% of the connected part, whereas for $\langle x \rangle_{u+d}$ the result is conisistent with zero giving an upper bound on the size of the disconnected contribution.

4. Results for 130 MeV $< m_\pi <$ 450 MeV

In this section we show results using a number of TMF ensembles for the axial charge, momentum fraction and scalar charge, including results for the physical ensemble.

As can be seen in Fig. 5, where results for g_A and $\langle x \rangle_{u-d}$ are displayed, our values at physical pion mass are consistent with the experimental ones, albeit with still large statistical error. A number of collaborations are currently engaging in systematic studies using simulations at near physical pion masses [15, 16, 17, 18, 14] and we therefore expect that the values of these key observables at the physical point will soon be more accurately determined. Having lattice results on the axial charge and the first moment of the unpolarized distribution we can examine the spin carried by quarks $J^q = \frac{1}{2}(A_{20}^q(0) + B_{20}^q(0))$. Both $A_{20}^q(Q^2)$ and $B_{20}^q(Q^2)$ are extracted from the nucleon matrix elements of $\mathcal{O}^{\mu_1\mu_2} = \bar{\psi}\gamma^{\{\mu_1} i \overleftrightarrow{D}^{\mu_2\}}\psi$ in the $\overline{MS}$ scheme at $\mu = 2$ GeV using non-perturbative renormalization.

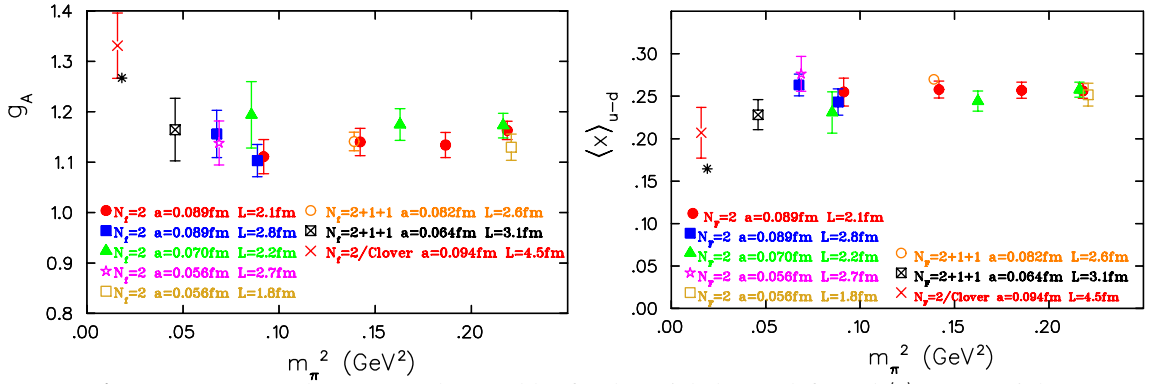

Figure 5: TMF results on several ensembles for the axial charge (left) and $\langle x \rangle_{u-d}$ [3] (right).

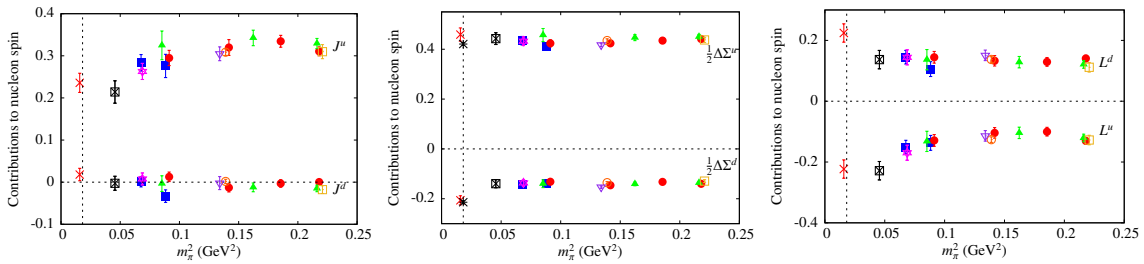

Figure 6: The spin $J^q = \frac{1}{2}\Delta\Sigma^q + L^q$ carried by the u and d quarks neglecting disconnected contributions except for B55.32 at $m_\pi = 373$ MeV, which includes the disconnected part (purple downward triangle).

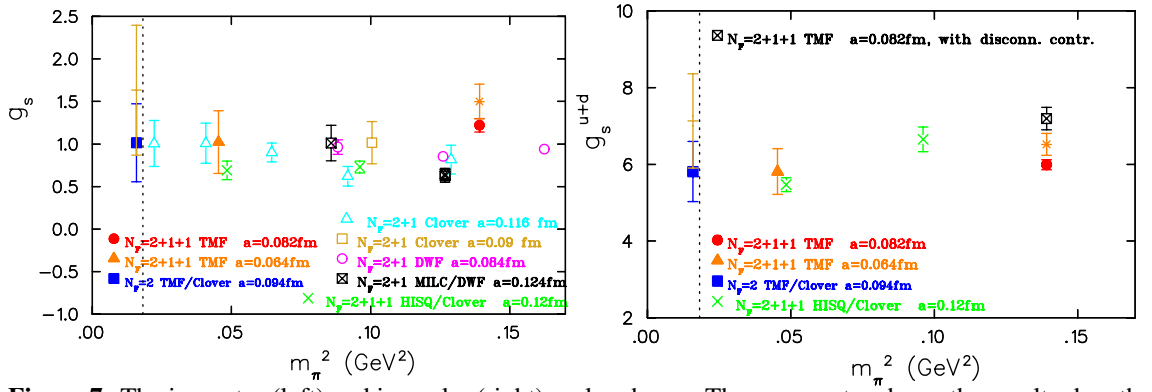

Figure 7: The isovector (left) and isoscalar (right) scalar charge. The orange star shows the result when the sink-source time separation is increased from 1.2 fm (filled circle) to ~ 1.5 fm for the B55.32 ensemble. The two points at the physical pion mass are obtained for $t_s = 1.1$ fm and 1.3 fm. The black square in the plot on the right panel includes the disconnected contribution.

In Fig. 4 we show the spin and angular momentum carried by the quarks in the nucleon. As can be seen, our preliminary results at the physical point are in agreement with experiment. A high statistics analysis of the disconnected contributions for the B55.32 ensemble shows a $\sim$10% contribution on $\Delta\Sigma^{u+d}$, which decreases its value as shown in Fig. 4, an effect that tends to bring its value towards the experimental one. In Fig. 7 we show the scalar charge computed for a sink-source time separation of 1 fm-1.2 fm. However, this observable has large excited state contamination and increasing t_s/a to 1.5 fm increases its value as shown in Fig. 7 for the B55.32 ensemble. The disconnected contribution, also computed for the B55.32 ensemble, increases its value further. It

is thus important, in order to obtain a reliable result, to perform the calculation at larger t_s/a and include the disconnected part.

5. Conclusions

Simulations at the physical point are now becoming available enabling results on g_A, $\langle x \rangle_{u-d}$ and other interesting observables directly at the physical point. High statistics and careful cross-checks of lattice artifacts will be needed to finalize these results. Noise reduction techniques such as the truncated solver method and all-mode-averaging will be crucial for future computations. Evaluation of disconnected quark loop diagrams has become feasible and disconnected contributions must be taken into account for observables such as the axial and scalar charges. Confirmation of experimentally known quantities such as g_A will enable reliable predictions of other less well-measured observables providing insight into the structure of hadrons and input that is crucial for new physics, such as the value of the nucleon σ-terms, the scalar and tensor charges.

Acknowledgements: Partial support was provided by the projects EPYAN/0506/08, TECHNOLOGY/ ΘΕΠΙΣ/0311(BE)/16 and ΠΡΟΣΕΛΚΥΣΗ/ΕΜΠΕΙΡΟΣ/0311/16 funded by the Cyprus Research Promotion Foundation, and by the EU ITN project PITN-GA-2009-238353 (ITN STRONGnet). This work used computational resources provided by PRACE, JSC, Germany and the Cy-Tera project (NEA ΥΠΟΔΟΜΗ/ΣΤΡΑΤΗ/0308/31).

References

[1] P. .Boucaud *et al.* [ETM Collaboration], Phys. Lett. B **650**, 304 (2007) [hep-lat/0701012]

[2] R. Baron, *et al.* [ETM Collaboration] JHEP **1006**, 111 (2010) [arXiv:1004.5284].

[3] C. Alexandrou *et al.* (ETMC) Phys. Rev. D **88**, 014509 (2013) [arXiv:1303.5979].

[4] R. Frezzotti and G. C. Rossi, JHEP **0408**, 007 (2004) [hep-lat/0306014].

[5] A. Abdel-Rehim *et al.* (ETMC), PoS Lattice 2013, 264 (2013).

[6] C. Alexandrou *et al.* [ETMC], Phys. Rev. D **83**, 045010 (2011) [arXiv:1012.0857].

[7] C. Alexandrou, Prog. Part. Nucl. Phys. **67**, 101 (2012) [arXiv:1111.5960].

[8] S. Dinter *et al.* (ETMC), Phys. Lett. B **704**, 89 (2011) [arXiv:1108.1076].

[9] C. Alexandrou *et al.* (ETMC), arXiv:1309.7768.

[10] C. Alexandrou, *et al.* (ETMC), arXiv:1309.2256.

[11] L. Maiani, G. Martinelli, M. L. Paciello and B. Taglienti, Nucl. Phys. B **293**, 420 (1987).

[12] A. Stathopoulos and K. Orginos, SIAM J. Sci. Comput. **32**, 439 (2010) [arXiv:0707.0131].

[13] S. Dinter *et al.* [ETM Collaboration], JHEP **1208**, 037 (2012) [arXiv:1202.1480].

[14] T. Bhattacharya, S. D. Cohen, R. Gupta, A. Joseph and H. -W. Lin, arXiv:1306.5435.

[15] J. R. Green *et al.*, arXiv:1209.1687.

[16] R. Horsley *et al.* (QCDSF), arXiv:1302.2233.

[17] S. Capitani *et al.* (CLS), Phys. Rev. D **86**, 074502 (2012) [arXiv:1205.0180].

[18] B. J. Owen *et al.*, Phys. Lett. B **723**, 217 (2013) [arXiv:1212.4668].